

Relativistic electron dynamics in intense crossed laser beams: Acceleration and Compton harmonics

Yousef I. Salamin*

*Theoretische Quantendynamik, Fakultät für Physik, Universität Freiburg, Hermann-Herder-Strasse 3, D-79104 Freiburg, Germany
and Physics Department, Birzeit University, P.O. Box 14-Birzeit, West Bank, Palestinian Authority*

Guido R. Mocken[†] and Christoph H. Keitel[‡]

*Theoretische Quantendynamik, Fakultät für Physik, Universität Freiburg, Hermann-Herder-Strasse 3, D-79104 Freiburg, Germany
(Received 9 November 2002; revised manuscript received 3 September 2002; published 8 January 2003)*

Electron motion and harmonic generation are investigated in the crossed-beam laser-accelerator scheme in a vacuum. Exact solutions of the equations of motion of the electron in plane-wave fields are given, subject to a restricted set of initial conditions. The trajectory solutions corresponding to axial injection are used to calculate precise emission spectra. Guided by hindsight from the analytic investigations, numerical calculations are then performed employing a Gaussian-beam representation of the fields in which terms of order ϵ^5 , where ϵ is the diffraction angle, are retained. Present-day laser powers and initial conditions on the electron motion that simulate realistic laboratory conditions are used in the calculations. The analytic plane-wave work shows, and the numerical investigations confirm, that an optimal crossing angle exists, i.e., one that renders the electron energy gain a maximum for a particular set of parameters. Furthermore, the restriction to small crossing angles is not made anywhere. It is also shown that energy gains of a few GeV and energy gradients of several TeV/m may be obtained using petawatt power laser beams.

DOI: 10.1103/PhysRevE.67.016501

PACS number(s): 52.75.Di, 42.65.-k, 52.38.-r, 42.50.Vk

I. INTRODUCTION

The scheme to accelerate electrons in vacuum by means of two crossed laser beams was proposed several years ago [1–3]. The basic idea here is to send the electron through the crossing point of two laser beams at an angle θ with respect to each beam direction (see Fig. 1 for a schematic and a coordinate system). Within the (simple) plane-wave picture and assuming the laser fields have the same amplitude and frequency, and are polarized as shown in Fig. 1, the resultant electric field component transverse to the electron initial direction of motion vanishes for all points on that axis. At the same time, the axial component works fully to accelerate the electron. The magnetic field component, on the other hand, vanishes at the same points. Thus subsequent motion of the electron, under these conditions, may be taken as linear. Esarey *et al.* [2] have derived working equations for the scheme employing a pair of linearly polarized laser beams, with Gaussian profiles, in the paraxial approximation, with acceleration mainly attributed to the forward electric field components of the beams. In their derivation various other approximations were employed, including the restriction to small intersection angles $\theta \ll 1$.

Later, Huang and his collaborators [4] used the equations of Esarey *et al.* in order to calculate parameters for dielectric-based, single-stage and multistage accelerator structures. Like other laser-accelerator schemes [3,5–7] this work is motivated by advances in laser technology [8–11],

which have recently led to the successful generation of sub-cycle pulses in the microwave [12], far-infrared [13], and femtosecond [14] regimes.

This paper may be considered as consisting of two parts. First, analytic work employing a plane-wave-based representation of the laser fields is presented which aims at: (a) a better understanding of the electron dynamics, (b) searching for deeper insights into the electron-field interaction and energy exchange, (c) calculating precise sample emission spectra based on the exact Liénard-Wiechert potentials of the electron, and (d) guiding the numerical work that follows. Second, results from numerical work, based on a realistic model of the laser fields in terms of those of a high-order Gaussian beam, are presented whose aim is to simulate the laboratory conditions as closely as possible when high-intensity laser fields are employed; a regime that requires

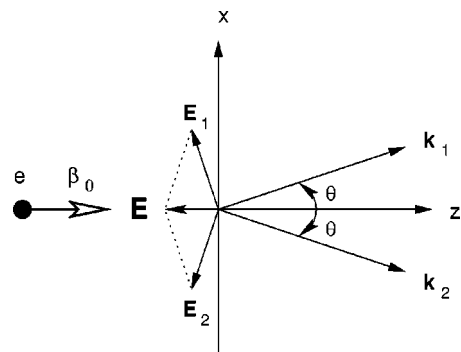


FIG. 1. Schematic diagram of the crossed-beam laser accelerator configuration. The electron, charge $-e$ and initial scaled speed β_0 , is injected along the z axis through the intersection point of the two beams. The plane-wave field polarizations are denoted by \mathbf{E}_1 and \mathbf{E}_2 and their propagation directions are given by \mathbf{k}_1 and \mathbf{k}_2 .

*Electronic address: ysalamin@birzeit.edu

[†]Electronic address: mocken@physik.uni-freiburg.de[‡]Electronic address: keitel@physik.uni-freiburg.de

focusing over small spatial dimensions. This will allow us to investigate stability of the electron motion under initial conditions less ideal than the forward injection case, by considering off-axis injection and injection at various initial speeds.

Chief among the results of the analytic work is the realization that, corresponding to any given set of field parameters, an optimum beam crossing angle exists which makes the electron energy gain a maximum. Furthermore, the radiative losses turn out to be small and the emission spectra exhibit the expected Doppler shifts, line enhancement, and tendency to be of approximately the same strength, all with increasing intensity. On the other hand, we learn from the numerical work that small deviations from initial forward injection result in considerable bending and large departure from linear motion. More importantly, energy gain, of several GeV from interaction with laser beams of laboratory intensities, is shown to be possible.

In the analytic work a set of working equations for the crossed-beam accelerator scheme are developed, employing the phase of the accelerating field as a variable. In terms of this variable, exact expressions for the electron energy and speed are obtained by direct integration of the relativistic equations of motion of the electron. An expression for the electron position as a function of the laser field phase is also obtained in terms of an integral which we carry out numerically for our purposes in this paper. Our equations are valid for all crossing angles and allow us to follow the subcycle evolution of the energy gradient, energy gain, speed, radiated power, and the time rate of change of energy gain during interaction with two different wave patterns, namely, a *strictly* plane-wave pattern and a pattern modeled by a \sin^2 envelope.

Although we investigate the electron dynamics during interaction with wave patterns containing several field cycles (in a sense to be described below), our analysis also suits situations in which a subcycle pulse may be used [15–17]. During a decelerating phase of the motion the electron speed may drop to zero and its direction of motion may be reversed, depending upon its initial injection energy. This leads to loss of energy through Bremsstrahlung and places limitations on the maximum energy attainable. In spite of that, for example, our numerical work shows that a maximum energy gain of about 1.9 GeV may be achieved using identical beams of 10 PW power focused down to 7 μm waist radii. This occurs for 2.555 MeV injected electrons and a crossing *half-angle* $\theta=3.1^\circ$. The acceleration to this energy takes place over an axial distance of less than 2 mm, which implies an energy gradient of nearly 1 TeV/m. The plane-wave-based calculations exaggerate these numbers by a factor of 2 or sometimes even much more.

The rest of this paper is organized as follows. In Sec. II we formulate the problem, modeling the laser fields by pulse-shape functions dependent entirely upon the laser field phase, and setting up the relevant equations of motion. This is followed by the analytic solution of the equations of motion and by a derivation of the evolution equations, in the said phase, of the electron dynamics. Next we investigate the radiative losses that accompany the motion of the electron in the laser fields and present examples of the emission spectra.

In Sec. III the most general description of the fields of a Gaussian beam are presented and then used to investigate several issues pertinent to the acceleration scheme. First the issue of a preferred crossing angle will be taken up. Using the preferred angles suggested by the numerical work, the effect (on the trajectories as well as on the energy gain) of a spread in the injection initial conditions, including the injection energies and positions, is discussed next. Finally, a summary of our main results and conclusions will be given in Sec. IV.

II. THE PLANE-WAVE ANALYSIS

A. Formulation of the problem

Referring to Fig. 1, we represent the propagation vectors of the two identical beams by $\mathbf{k}_1 = \omega/c(\hat{\mathbf{i}} \sin \theta + \hat{\mathbf{k}} \cos \theta)$ and $\mathbf{k}_2 = (\omega/c)(-\hat{\mathbf{i}} \sin \theta + \hat{\mathbf{k}} \cos \theta)$, where ω is the laser frequency, c is the speed of light in vacuum, and $\hat{\mathbf{i}}$, $\hat{\mathbf{j}}$, and $\hat{\mathbf{k}}$ are unit vectors in the directions of increasing x , y , and z , respectively. Let the phases of the fields at any space-time point (t, \mathbf{r}) be given by $\eta_1 = \omega t - \mathbf{k}_1 \cdot \mathbf{r}$, and $\eta_2 = \omega t - \mathbf{k}_2 \cdot \mathbf{r}$. Introducing $g(\eta_j)$ as an envelope function for the j th beam and assuming the beams have the same amplitude E_0 , the electric and magnetic fields of the two beams are

$$\mathbf{E}_1 = E_0 g(\eta_1) \cos \eta_1 (\hat{\mathbf{i}} \cos \theta - \hat{\mathbf{k}} \sin \theta), \quad (1)$$

$$\mathbf{E}_2 = -E_0 g(\eta_2) \cos \eta_2 (\hat{\mathbf{i}} \cos \theta + \hat{\mathbf{k}} \sin \theta), \quad (2)$$

$$\mathbf{B}_1 = E_0 g(\eta_1) \cos \eta_1 \hat{\mathbf{j}}, \quad (3)$$

$$\mathbf{B}_2 = -E_0 g(\eta_2) \cos \eta_2 \hat{\mathbf{j}}. \quad (4)$$

Note that the \mathbf{E} and \mathbf{B} fields given in Eqs. (1)–(4) satisfy Maxwell's equations. We employ these equations in the exploratory analytic work.

Utilizing the axial symmetry of the problem, the transverse motion of the electron may be neglected for electrons injected exactly axially (along z). This will receive solid support and full justification from the numerical work of Sec. III. Under these conditions, $\eta_1, \eta_2 \rightarrow \eta = \omega[t - (z/c) \cos \theta]$. Moreover, the resultant magnetic field vanishes for all points on the z axis, while the resultant electric field has only a nonvanishing axial component given by

$$E_z(0,0,z) = -2E_0 g(\eta) \sin \theta \cos \eta. \quad (5)$$

This accelerating field has an amplitude $2E_0 \sin \theta g(\eta)$, a phase η , and hence, a phase velocity $v_{ph} = c/\cos \theta > c$. Henceforth, but within the plane-wave context, *one (accelerating) field cycle* will mean $\eta = 2\pi$. Since the speed of the electron can never exceed c it will phase-slip behind the accelerating field. In the remainder of this section η will be used as a variable in terms of which all physical quantities of relevance will be written and discussed. Our analysis of the electron dynamics will cover several integer values of $\eta/2\pi$ [15–17]. In a practical situation, the interaction will be confined to a region of space around the origin whose size de-

pends on the shape and size of the beam cross section at focus. Hence the electron will practically interact with a fraction of a cycle of the accelerating field, or a few such cycles at most, depending upon the parameters used. Chief among those parameters are the beam waist radii, the Rayleigh lengths, and the crossing angle.

Let the electron have a mass m and a charge $-e$. A solution to the following equations of motion will now be developed ($\mathbf{E}=\mathbf{E}_1+\mathbf{E}_2$ and $\mathbf{B}=\mathbf{B}_1+\mathbf{B}_2$)

$$\frac{d\mathbf{p}}{dt} = -e(\mathbf{E} + \boldsymbol{\beta} \times \mathbf{B}), \quad \frac{d\mathcal{E}}{dt} = -ec\boldsymbol{\beta} \cdot \mathbf{E}. \quad (6)$$

In Eq. (6) $\mathbf{p} = \gamma mc \boldsymbol{\beta}$ is the relativistic momentum of the electron and $\mathcal{E} = \gamma mc^2$ is its energy, where $\boldsymbol{\beta}$ is the velocity vector normalized by the speed of light and $\gamma = (1 - \beta^2)^{-1/2}$ is the Lorentz factor. With $\boldsymbol{\beta} = (\beta_x, \beta_y, \beta_z)$, the exact equations of motion are equivalent to four component ones. The x - and y -component equations result in no motion due to the vanishing of the magnetic field on the z axis. The remaining two equations then take the form

$$\frac{d(\gamma\beta_z)}{dt} = 2q\omega \sin \theta g(\eta) \cos \eta, \quad (7)$$

$$\frac{d\gamma}{dt} = 2q\omega \sin \theta g(\eta) \beta_z \cos \eta, \quad (8)$$

where we have introduced $q = eE_0/(mc\omega)$ as a convenient dimensionless intensity parameter. Recall that

$$I\lambda^2 = \left(\frac{mc^2}{e}\right)^2 \left(\frac{\pi c}{2}\right)^2 q^2 \approx 1.375 \times 10^{18} q^2 (\text{W/cm}^2)(\mu\text{m})^2. \quad (9)$$

Equation (9) will be employed in computing the intensities used in Figs. 6 and 7.

B. Electron dynamics

It will be assumed that the electron is sent initially along the z axis at the scaled speed β_0 , and that it will be overcome by the front edges of the crossed laser beams simultaneously at time $t=0$, at the origin of coordinates. The electron *energy gain*, as a result of interaction with $\eta/2\pi$ cycles of the accelerating field, may be defined by

$$W(\eta) \equiv mc^2[\gamma(\eta) - \gamma_0]. \quad (10)$$

With the help of Eq. (8), the following expression may be obtained for the *energy gradient* (energy gained per unit interaction distance) as a function of the accelerating field phase

$$G(\eta) \equiv \frac{dW}{dz} = mc^2 \frac{d\gamma}{dz} = 2qmc\omega g(\eta) \sin \theta \cos \eta. \quad (11)$$

The energy gradient is proportional to the accelerating field [compare Eqs. (5) and (11)]. We show $G(\eta)$ in Fig. 2.

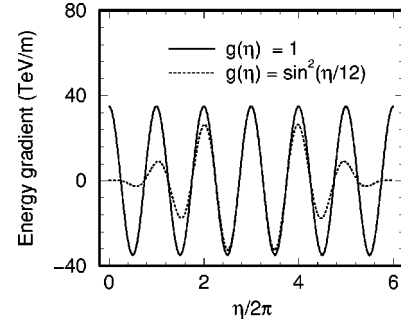


FIG. 2. Energy gradient vs the number of cycles of the accelerating field. The parameters are: $\lambda = 1.056 \mu\text{m}$, $\theta = 3.2^\circ$, and $q = 102.622$ [laser power = 10 PW, see Eq. (46) below].

The solid line in Fig. 2 represents a plane wave, $g(\eta) = 1$, while the dotted line is for a wave pattern having a \sin^2 envelope given by

$$g(\eta) = \sin^2\left(\frac{\kappa\eta}{2}\right), \quad (12)$$

where $0 < \kappa < 1$. For example, for $\kappa = 1/6$ this pulse-shape function envelopes a pattern of 6 field cycles.

From Fig. 2 one finds out that $G(\eta)$ is positive during one half cycle and negative during the following half cycle. Thus, for interaction with an integer number of field cycles, the energy gains tend to get canceled by the energy losses, in agreement with the Lawson-Woodward theorem [18]. Our analysis will cover interaction with a full field pattern, or pulse in this effectively one-dimensional model. For the purpose of acceleration, the assumption is that the electron may be ejected from the region of interaction while it still retains part or all of the energy gained.

We also conclude from studying Fig. 2 that both pulse-shapes considered present the electron with the same field in the small region around the focus. Thus it does not matter which envelope function we use in our theoretical investigations of the electron dynamics in that region.

In an accelerator design one would want to know where exactly will the electron have what energy. In order to reach this goal we set out now to find the energy gain $W(\eta)$ and the coordinate of the electron along the forward direction of motion $z(\eta)$. We will display graphically the gain W against z using their respective expressions as parametric equations in terms of η , regarded as the parameter.

Since motion is confined to one dimension, we will drop the subscript z from this point on. Differentiating the field phase with respect to the time variable gives

$$\frac{d\eta}{dt} = \omega(1 - \beta \cos \theta). \quad (13)$$

Carrying out the differentiation with respect to time explicitly on the left hand side of Eq. (7), the time dependence may be eliminated in favor of dependence upon the field phase η with the help of Eqs. (8) and (13). Separation of the (new) variables next gives

$$\frac{(1 - \beta \cos \theta)}{(1 - \beta^2)^{3/2}} d\beta = 2qg(\eta) \sin \theta \cos \eta d\eta. \quad (14)$$

Integration subject to the above mentioned initial conditions finally yields

$$\gamma(\beta - \cos \theta) = \gamma_0(\beta_0 - \cos \theta) + 2qf(\eta) \sin \theta \equiv s(\eta), \quad (15)$$

where

$$f(\eta) = \int_{\eta_0}^{\eta} g(\eta') \cos \eta' d\eta'. \quad (16)$$

For book-keeping purposes note that for the plane-wave and \sin^2 patterns one has ($\eta_0 = 0$)

$$f(\eta) = \sin \eta, \quad (17)$$

and

$$f(\eta) = \frac{\sin \eta}{2} - \frac{\sin[(1 + \kappa)\eta]}{4(1 + \kappa)} - \frac{\sin[(1 - \kappa)\eta]}{4(1 - \kappa)}, \quad (18)$$

respectively.

Equation (15) may now be solved for the electron velocity scaled by the speed of light

$$\beta(\eta) = \frac{\cos \theta + s \sqrt{s^2 + \sin^2 \theta}}{1 + s^2}. \quad (19)$$

Alternatively, Eq. (15) may be solved for the electron energy scaled by mc^2 ,

$$\gamma(\eta) = \frac{s \cos \theta + \sqrt{s^2 + \sin^2 \theta}}{\sin^2 \theta}. \quad (20)$$

Equations (19) and (20) have the correct limits. Consider the case of $\theta=0$, for example. This case corresponds to two co-propagated beams. For the chosen polarizations, however, the electric fields cancel out at all time and, hence, subsequent motion of an electron that has initially been injected exactly along the z axis should not be affected by such fields. Note that setting $\theta=0$ in Eq. (15) gives $s = -\gamma_0(1 - \beta_0) < 0$. When this result is used in Eqs. (19) and (20), and provided the square roots are handled with care, one finds out that $\beta(\eta) \rightarrow \beta_0$ and $\gamma(\eta) \rightarrow \gamma_0$, as they should.

With Eq. (20) for the scaled energy we can now discuss the energy gain $W(\eta)$, defined by Eq. (10). We begin by showing this quantity in Figs. 3(a) and 3(b) for two different pulse-shape envelopes. Due to the fact that each of the envelope functions is normalized to have a unit maximum height at focus, the energy gain has the same maximum value for both of them. Note that in all cases all gain is lost as the electron is left behind the pattern, in agreement with the Lawson-Woodward theorem. This is due essentially to the inherent symmetry of the plane-wave model. This symmetry gets destroyed by focusing over small spatial dimensions, and a net gain becomes possible, as will be demonstrated in

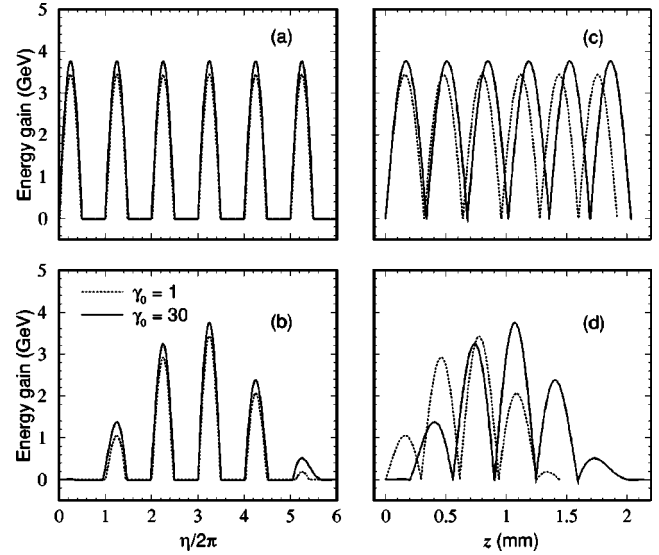


FIG. 3. Electron energy gain vs the number of accelerating field cycles and also vs the forward distance of travel z . (a) and (c): The plane-wave pattern, and (b) and (d): The wave pattern with a \sin^2 pulse shape. The remaining field parameters are the same as those of Fig. 2.

Sec. III. Moreover, the gain increases during, say, the first quarter of a field cycle and the electron is accelerated. The gain reaches a maximum at the end of the first quarter cycle and then drops down during interaction with the second quarter cycle. The Lorentz factor γ changes a little from unity during interaction with the next half cycle (dotted line, electron initially at rest). This explains the flat portion (actually concave upward) of W vs $\eta/2\pi$ between the $\eta/2\pi = 0.5$ and 1 marks in the dotted line of Fig. 3(a). In fact, the Lorentz factor reaches a value less than γ_0 (solid line, $\gamma_0 = 30$) and drops down to unity as $\beta \rightarrow 0$ in this region, and W becomes slightly negative there. This may be better understood by studying Fig. 5 for the scaled speed, where it is shown that the electron slows down and reverses its direction of motion.

Another important point to note in Fig. 3 is that the electron is accelerated from rest to a maximum of about 3.4 GeV and from roughly 15 MeV to a little over 3.8 GeV. Both results are achieved regardless of what pulse-shape function $g(\eta)$ is used to model the field of 10 PW power. This will be shown to be about twice the gain obtained numerically from the Gaussian-beam-based calculation. Only at a plane right through its focus, $z=0$, (and too far away from focus, where the intensity may be negligible anyway) does a Gaussian-beam exhibit plane-wave characteristics.

Of more interest to the experimentalist would be to see a display of W vs z . To produce such a figure we need an expression for the axial electron coordinate $z(\eta)$ which we now derive. Using the chain rule of differentiation and employing Eqs. (13) and (19) we get

$$\frac{dz}{d\eta} = \frac{dz}{dt} \frac{dt}{d\eta} = \frac{c}{\omega} \frac{\beta(\eta)}{[1 - \beta(\eta) \cos \theta]}. \quad (21)$$

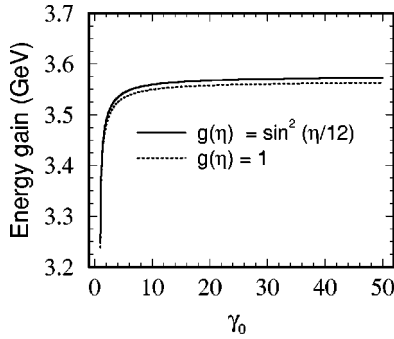


FIG. 4. The maximum energy gain (calculated for $\eta/2\pi=3.2$) is seen here to saturate with increasing initial injection energy. The parameters used are the same as in Fig. 2.

The remaining integration in Eq. (21) will be carried out numerically, for the sake of the discussion below. We show W vs z in Figs. 3(c) and 3(d). Note the presence of what looks like cusps in these plots. In fact, each of these cusp-looking portions is a tiny loop, too small to show on the scale used. Inspection of the data used to produce, say the dotted line in Fig. 3(c), reveals a turning point in the trajectory the electron reaches as its speed drops to zero. It then turns around, moves a fraction of $1 \mu\text{m}$ to the left to another turning point and then speeds up to the right again. Over the loop structure the electron moves at speeds too small compared to the speed of light, which explains why it hardly moves forward (or backward) during interaction with about half of a (mostly decelerating) field cycle.

The examples considered in Fig. 3 exhibit large average acceleration gradients. Ejection at the top of the first hump of each line in Fig. 3(a), for example, achieves average energy gradients of roughly 25 TeV/m (solid line) and 23 TeV/m (dotted line).

The initial conditions laid down above are admittedly artificial, somehow. We have simply stated that the electron is *born* at the origin of coordinates at $t=0$ inside the plane wave which, by definition, has an infinite extension in both space and time. Figure 3 suggests that such an electron stands to gain more energy from the field if it *starts off* at a higher speed. Figure 4 shows this to be indeed the case but not indefinitely. The gain exhibits saturation (at about 3.575 GeV, for the parameters used) after an initial steep rise, with increasing injection energy.

The sinusoidal dependence upon η of the scaled speed [cf. Eqs. (15)–(19)] shows clearly in the oscillations displayed in Fig. 5. The scaled speed drops from a relativistic value close to unity down to zero and even becomes negative, as the field changes direction and works to decelerate the electron. The minimum (negative) value reached by β depends, of course, on the value of β_0 although this may not be seen in Fig. 5 because in it we employ parameters of an extremely powerful laser system. In such an environment the acceleration to ultrarelativistic speeds takes place quite swiftly.

We conclude this section by noting that in a recent letter Salamin and Keitel [3] have studied this electron-field configuration employing $\sin \eta$ plane-wave fields and allowing for interaction with only half of a field cycle. An important

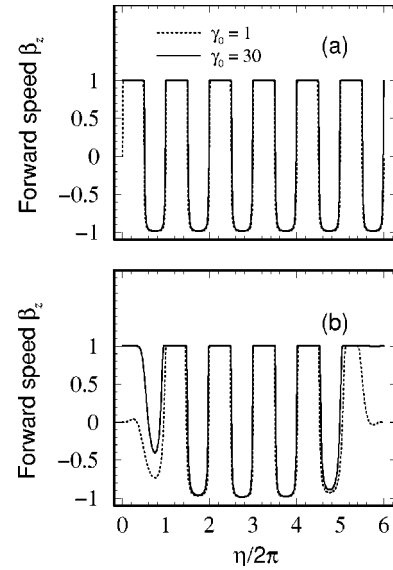


FIG. 5. Forward scaled speed of the electron vs the number of accelerating field cycles. (a) Plane-wave pattern, and (b) \sin^2 pattern. The field parameters used are the same as in Fig. 2.

outcome of that work was the demonstration that an optimum crossing angle, one that makes the overall gain a maximum, exists for each set of chosen parameters. More on this issue will be found in Sec. III below.

C. Radiative losses

Electron motion in the scheme of acceleration by crossed laser beams is essentially linear, provided injection is perfectly axial. It is well-known [19] that radiative losses in a linear accelerator are negligibly small.

However, this is a fact if the particle undergoes steady acceleration. As may be seen in Fig. 5, the electron speed in this scheme oscillates: it becomes extremely relativistic in the forward direction as the electron absorbs energy from the field and then it falls down to zero and even becomes negative, depending upon its injection value. During deceleration the electron loses substantial energy through Bremsstrahlung. We now investigate the radiative losses employing the relativistic version of the Larmor formula for the radiated power [19]

$$P(t) = \frac{2}{3} \frac{e^2}{c} \gamma^6 \left\{ \left[\frac{d\boldsymbol{\beta}}{dt} \right]^2 - \left[\boldsymbol{\beta} \times \frac{d\boldsymbol{\beta}}{dt} \right]^2 \right\}. \quad (22)$$

For motion along a straight line, the second term in Eq. (22) vanishes. Equation (14) may then be used to write the expression for the radiated power as a function of the accelerating field phase

$$P(\eta) = \frac{2}{3} \frac{e^2}{c} [2q\omega g(\eta) \sin \theta \cos \eta]^2. \quad (23)$$

Equation (23) gives the rate at which energy is lost by the electron through radiation. This quantity should be compared with the rate at which the electron gains energy by absorption from the field. The rate of energy gain is

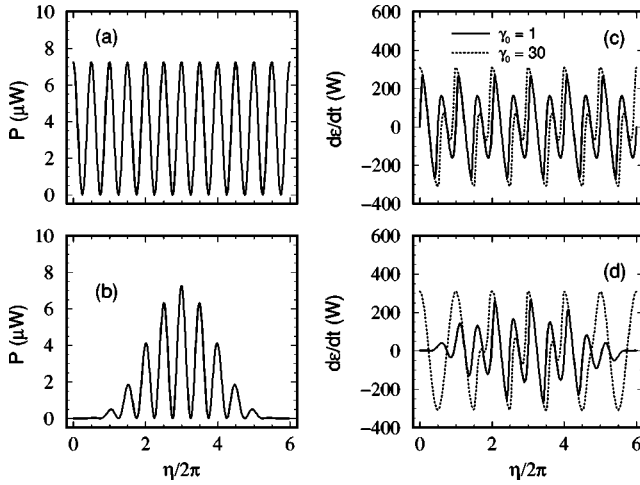


FIG. 6. The radiated power and the rate of change of the electron energy vs the number of accelerating field cycles. The initial electron scaled injection energies are $\gamma_0=1$ (solid lines) and $\gamma_0=30$ (dotted lines). Note the solid and dotted lines coincide in (a) and (b) on account of the fact that $P(\eta)$ is independent of β_0 . (a) and (c) are for the plane-wave pattern $g(\eta)=1$, while (b) and (d) are for the pattern with $g(\eta)=\sin^2(\eta/12)$. The field parameters are: $\lambda=1 \mu\text{m}$, $q=10$, or $I=1.375 \times 10^{20} \text{ W cm}^{-2}$ [see Eq. (9)], and $\theta=0.1 \text{ rad}$.

$$\frac{dW}{dt} = \frac{d\mathcal{E}}{dt} = mc^2 [2q\omega g(\eta) \sin \theta \cos \eta] \beta(\eta), \quad (24)$$

from Eqs. (8) and (10). Construction of the ratio of $P(\eta)$ to dW/dt runs into difficulty due to the fact that the latter vanishes at several values of η .

We show these quantities separately in Fig. 6 for interaction with a field of intensity of $1.375 \times 10^{20} \text{ W/cm}^2$ [$q=10$, according to Eq. (9)] and employing the pulse-shape functions used in Figs. 2–5. In the small regions of η space corresponding to deceleration, the ratio of P_{max} to $(dW/dt)_{max}$ can be non-negligible (a few percent) as the electron loses part of the gained energy by radiation. Elsewhere, during acceleration, the same ratio becomes negligibly small, typically less than 10^{-7} . Our single-particle analysis gets a little modified when the bunch characteristics are taken into account by introduction of suitable bunch form factors [20].

D. Emission spectra

We have seen in the previous subsections that the electron undergoes violent acceleration and deceleration in the fields of two crossed laser beams. It has also been demonstrated that the resulting radiative losses can be non-negligible. We devote this section to a study of the emission spectra of the free electron in the prescribed fields. Production of harmonics of the incident radiation field, for free [21–32] and bound [33–40] electrons is an active area of investigation. It has also been shown recently [20] that characteristics of the emitted radiation may be used as a valuable tool for electron bunch diagnosis, a tool that does not involve intercepting or deflecting the electron beam substantially.

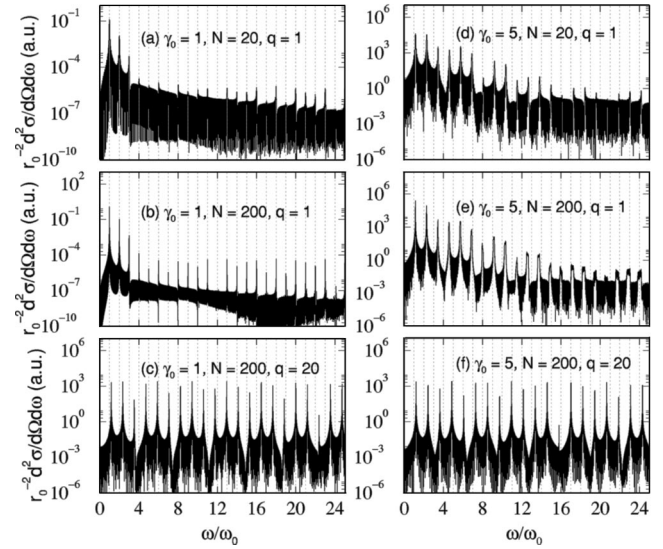


FIG. 7. (Color online). Sample emission spectra of an electron initially at rest ($\gamma_0=1$) at the origin or with initial speed ($\gamma_0=5$) along the z axis and subsequently subjected to two crossed laser beams ($\theta=0.1 \text{ rad}$) modeled by plane-wave patterns ($g(\eta)=1$) with $\lambda=1 \mu\text{m}$. The observation point is in the xz plane and located by polar angles $\Theta=80 \text{ mrad}$ and $\Phi=0$. The calculation has been carried out for interaction with N field cycles and using intensity parameters $q=1$ ($I \approx 1.375 \times 10^{18} \text{ W/cm}^2$) and $q=20$ ($I \approx 5.5 \times 10^{20} \text{ W/cm}^2$). The intensities were calculated using Eq. (9).

In this section we will be using ω to denote the generated frequency and ω_0 to denote the laser frequency. Although, the spectra to be shown in Fig. 7 are calculated using the exact Liénard-Wiechert potentials, we employ the following equation, as a starting point for the discussion [19] (far field approximation)

$$\frac{d^2E(\omega, \Omega)}{d\Omega d\omega} = \frac{e^2}{4\pi^2 c} \left| \int_0^T \frac{\hat{n} \times [\hat{n} - \boldsymbol{\beta}(t)] \times \dot{\boldsymbol{\beta}}(t)}{[1 - \hat{n} \cdot \boldsymbol{\beta}(t)]^2} \times \exp \left\{ i\omega \left[t - \frac{\hat{n} \cdot \mathbf{r}(t)}{c} \right] \right\} dt \right|^2. \quad (25)$$

In Eq. (25) E is temporarily used to denote the radiated energy, \hat{n} is a unit vector in the direction of propagation of the emitted radiation (direction of observation), $\dot{\boldsymbol{\beta}}$ is the particle acceleration scaled by the speed of light, and T is used temporarily to denote the time interval over which interaction between the electron and the laser field takes place. Equation (25) holds as long as the dimensions of the electron trajectory are much smaller than the distance from the electron to the observation point. This has been demonstrated quite well by the trajectory analysis given above. In what follows, a spectrum will be reported in terms of the doubly-differential scattering cross section, given by

$$\frac{d^2\sigma(\omega, \Omega)}{d\Omega d\omega} = \frac{1}{T} \frac{8\pi c r_0^2}{(eq\omega_0)^2} \frac{d^2E(\omega, \Omega)}{d\Omega d\omega}. \quad (26)$$

Equation (26) has been obtained by dividing the radiant energy, emitted into a unit solid angle per unit frequency per unit time, by the incident energy flux (of one beam), $(eq\omega_0)^2/8\pi cr_0^2$, r_0 being the classical electron radius. An integration by parts may next be performed on Eq. (25) which when followed by a change of variable from t to $\eta = \omega_0[t - (z/c)\cos\theta]$ results in (atomic units, with $e = m = 1$, are used)

$$\frac{1}{r_0^2} \frac{d^2\sigma(\omega, \Omega)}{d\Omega d\omega} = \frac{\omega_0}{N(q\pi\omega_0)^2} \left| \mathbf{U}(\omega) - i \left(\frac{\omega}{\omega_0} \right) \mathbf{V}(\omega) \right|^2, \quad (27)$$

where

$$\begin{aligned} \mathbf{U}(\omega) &= \left[\frac{\hat{\mathbf{n}} \times \hat{\mathbf{n}} \times \boldsymbol{\beta}(\eta)}{1 - \hat{\mathbf{n}} \cdot \boldsymbol{\beta}(\eta)} \exp \left\{ i \frac{\omega}{\omega_0} \left[\eta + \frac{\omega_0}{c} [z \cos \theta - \hat{\mathbf{n}} \cdot \mathbf{r}(\eta)] \right] \right\} \right] \Bigg|_0^{2\pi N} \\ &= [(n_1 n_3) \hat{\mathbf{i}} + (n_2 n_3) \hat{\mathbf{j}} + (n_3^2 - 1) \hat{\mathbf{k}}] \\ &\quad \times \left[\frac{\beta}{1 - n_3 \beta} \exp \left\{ i \frac{\omega}{\omega_0} \left[\eta + \frac{\omega_0}{c} z (\cos \theta - n_3) \right] \right\} \right]_0^{2\pi N}, \end{aligned} \quad (28)$$

$$\begin{aligned} \mathbf{V}(\omega) &= \frac{\omega_0}{c} \int_0^{2\pi N} \left[\hat{\mathbf{n}} \times \hat{\mathbf{n}} \times \frac{d\mathbf{r}}{d\eta} \exp \left\{ i \frac{\omega}{\omega_0} \left[\eta + \frac{\omega_0}{c} [z \cos \theta - \hat{\mathbf{n}} \cdot \mathbf{r}(\eta)] \right] \right\} \right] d\eta \\ &= \frac{\omega_0}{c} [(n_1 n_3) \hat{\mathbf{i}} + (n_2 n_3) \hat{\mathbf{j}} + (n_3^2 - 1) \hat{\mathbf{k}}] \\ &\quad \times \int_0^{2\pi N} \frac{dz}{d\eta} \exp \left\{ i \frac{\omega}{\omega_0} \left[\eta + \frac{\omega_0}{c} z (\cos \theta - n_3) \right] \right\} d\eta. \end{aligned} \quad (29)$$

Note that in the second equalities of Eqs. (28) and (29) the subscript has been dropped from β_z . Furthermore, location of the observation point will be given in spherical polar coordinates, i.e., $\hat{\mathbf{n}} = (n_1, n_2, n_3) = (\sin \Theta \cos \Phi, \sin \Theta \sin \Phi, \cos \Theta)$. The coordinate system is the same as that of Fig. 1, in which Θ is measured relative to the positive z axis and Φ relative to $+x$. It should be mentioned that the integration in Eq. (25) has a highly oscillating integrand, which makes the calculation quite laborious. Obviously, no radiation is expected to be emitted along the forward and backward directions, $\Theta = 0$ and π , respectively, as both \mathbf{U} and \mathbf{V} may be seen to vanish identically in these cases.

Sample emission spectra, calculated numerically using the exact version [19] of Eq. (25), are shown in Fig. 7 for an observation point in the xz plane, $\Phi = 0$. Interaction times equivalent to 20 and 200 field cycles have been taken. Reasonably sharp spectral lines have been produced. In addition

to the emission at the fundamental (pump) frequency, over 20 harmonics could be calculated with reasonable accuracy. Note that the lines are Doppler shifted to the right of their expected positions (integer values of ω/ω_0) as the source, the electron, reaches relativistic speeds. This is most evident in the cases where high-intensity incident light is scattered from electrons injected with high initial momenta.

On the other hand, in the presence of high-intensity fields, the role of the initial momentum in determining the strength of the lines, and the overall shift in their positions, diminishes. Thus lines of comparable strength, and overall shift, result for both cases of electron initially at rest, Fig. 7(c), and one that is initially incident with high velocity, Fig. 7(f).

III. THE GAUSSIAN-BEAM ANALYSIS

We have presented an analysis of the dynamics of a single electron in vacuum in the field of two laser beams crossing at an angle, using a set of exact equations stemming from an analytic solution to the equations of motion of the electron in the plane-wave fields. No restrictions have been made on the value of the crossing angle or laser field intensity. Practical considerations, however, may place severe limits on the range of values of θ and q in a realistic accelerator design. If conditions allow the electron to interact with a large number of field cycles, the length of the accelerator unit increases dramatically. An ideal situation would be to confine the interaction to one half of a field cycle [3] by suitably choosing the crossing angle and the field parameters (especially spot size). On the other hand, arbitrarily high field intensities, essential for achieving the desired high electron energies, may be difficult to use due to the damage they may cause to the optical components needed for the design. In any case expert knowledge in mirror material and the breakdown mechanism will be required to make an arrangement work.

In order to be able to achieve the desired high-energy gains, an investigation of the electron dynamics ought to be conducted in the relativistic regime of laser intensities. On the other hand, the required high intensity-laser fields can only be realized by focusing over small dimensions. Thus, a detailed knowledge of the laser electric and magnetic fields near the focus of the Gaussian beam is essential [41–45]. This is done next.

A. The fields

In the Gaussian description of a focused laser beam, the plane-wave symmetry is destroyed and the beam develops field components along the three spatial directions. For the acceleration scheme of interest to us in this paper, we employ the coordinate system shown in Fig. 8(a). Subscripts 1 and 2 are used to label the beams. Like in the plane-wave case, the x 's and z 's are taken in the plane of the paper, while the y 's point out of it. It is easy to demonstrate that the coordinates obey the following transformation relations

$$x_1 = x \cos \theta - z \sin \theta, \quad y_1 = y, \quad z_1 = x \sin \theta + z \cos \theta, \quad (30)$$

$$x_2 = -x \cos \theta - z \sin \theta, \quad y_2 = y, \quad z_2 = -x \sin \theta + z \cos \theta. \quad (31)$$

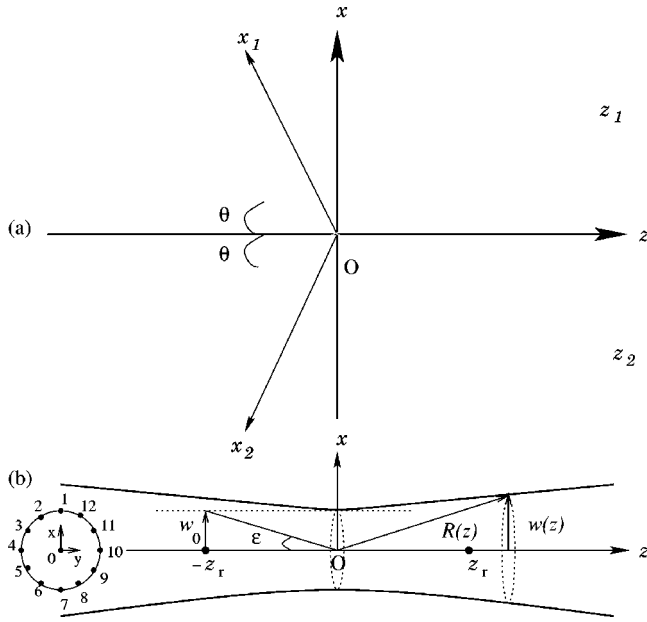


FIG. 8. (Color online). (a) Coordinate system employed in the Gaussian-beam analysis. The field propagation directions are along z_1 and z_2 , E_{1x} and E_{2x} point along x_1 and x_2 , respectively, and y_1 and y_2 are out of the page (and y_2 is into the page) through the common coordinate origin at O. (b) Geometry of the Gaussian beam (see the text for explanations). On the circle on the left hand side of (b) the dots mark the initial positions, in the xy plane, of 13 electrons; one at the center and 12 evenly distributed on the circumference, whose motion and energetics we discuss in Figs. 11–13.

Geometry of a Gaussian beam is shown in Fig. 8(b). The beam axis is taken along z , with its propagation direction along $+z$ and *stationary* focus at the origin of coordinates O. The beam cross section at focus is circular and has a radius w_0 ; a cross section at an arbitrary z is also circular with radius $w(z) = w_0 \sqrt{1 + (z/z_r)^2}$. Furthermore, $z_r = kw_0^2/2$ is the Rayleigh length, and $\epsilon = w_0/z_r$ is the diffraction angle. Now, letting $\xi = x/w_0$, $v = y/w_0$, and $\zeta = z/z_r$, the electric components of the laser field associated with such a beam, to order ϵ^5 , are [41,42,44,46,47]

$$E_x = E \left\{ S_0 + \epsilon^2 \left[\xi^2 S_2 - \frac{\rho^4 S_3}{4} \right] + \epsilon^4 \left[\frac{S_2}{8} - \frac{\rho^2 S_3}{4} - \frac{\rho^2(\rho^2 - 16\xi^2)S_4}{16} - \frac{\rho^4(\rho^2 + 2\xi^2)S_5}{8} + \frac{\rho^8 S_6}{32} \right] \right\}, \quad (32)$$

$$E_y = E \xi v \left\{ \epsilon^2 [S_2] + \epsilon^4 \left[\rho^2 S_4 - \frac{\rho^4 S_5}{4} \right] \right\}, \quad (33)$$

$$E_z = E \xi \left\{ \epsilon [C_1] + \epsilon^3 \left[-\frac{C_2}{2} + \rho^2 C_3 - \frac{\rho^4 C_4}{4} \right] + \epsilon^5 \left[-\frac{3C_3}{8} - \frac{3\rho^2 C_4}{8} + \frac{17\rho^4 C_5}{16} - \frac{3\rho^6 C_6}{8} + \frac{\rho^8 C_7}{32} \right] \right\}. \quad (34)$$

Similarly, the magnetic field components are given by

$$B_x = 0, \quad (35)$$

$$B_y = E \left\{ S_0 + \epsilon^2 \left[\frac{\rho^2 S_2}{2} - \frac{\rho^4 S_3}{4} \right] + \epsilon^4 \left[-\frac{S_2}{8} + \frac{\rho^2 S_3}{4} + \frac{5\rho^4 S_4}{16} - \frac{\rho^6 S_5}{4} + \frac{\rho^8 S_6}{32} \right] \right\}, \quad (36)$$

$$B_z = E v \left\{ \epsilon [C_1] + \epsilon^3 \left[\frac{C_2}{2} + \frac{\rho^2 C_3}{2} - \frac{\rho^4 C_4}{4} \right] + \epsilon^5 \left[\frac{3C_3}{8} + \frac{3\rho^2 C_4}{8} + \frac{3\rho^4 C_5}{16} - \frac{\rho^6 C_6}{4} + \frac{\rho^8 C_7}{32} \right] \right\}. \quad (37)$$

In Eqs. (32)–(37), we have taken

$$E = E_0 \frac{w_0}{w} g(\eta) \exp \left[-\frac{r^2}{w^2} \right], \quad (38)$$

$$S_n = \left(\frac{w_0}{w} \right)^n \sin(\psi + n\psi_G), \quad (39)$$

$$C_n = \left(\frac{w_0}{w} \right)^n \cos(\psi + n\psi_G). \quad (40)$$

Furthermore, $k = \omega/c$, $kA_0 = E_0$, $r^2 = x^2 + y^2$, and $\rho = r/w_0$. For a continuous beam with a stationary focus we will take $g(\eta) = 1$ in this work. For more of the details of the calculation leading to Eqs. (32)–(37) see the Appendix in Ref. [47]. These equations were derived from a vector potential polarized along x , has an amplitude A_0 , and a frequency ω . The remaining symbols in Eqs. (32)–(37) have the following definitions

$$\psi = \psi_0 + \psi_P - \psi_R + \psi_G, \quad (41)$$

$$\psi_P = \omega t - kz, \quad (42)$$

$$\psi_G = \tan^{-1} \zeta, \quad (43)$$

$$\psi_R = \frac{kr^2}{2R}, \quad (44)$$

$$R(z) = z + \frac{z_r^2}{z}. \quad (45)$$

Note that ψ_0 is a constant, $\psi_P = \eta$ is the plane wave phase, ψ_G is the Guoy phase associated with the fact that a Gaussian-beam undergoes a total phase change of π as z changes from $-\infty$ to $+\infty$, ψ_R is the phase associated with the curvature of the wave fronts, and that $R(z)$ is the radius of curvature of a wave-front intersecting the beam axis at the coordinate z . The fields given above satisfy Maxwell's equations $\nabla \cdot \mathbf{E} = 0 = \nabla \cdot \mathbf{B}$, plus terms of order ϵ^6 [46,47].

A laser system is often characterized by its output power P . For the fields given by Eqs. (32)–(37) the power may be calculated by integrating the time-averaged Poynting vector

over a plane through the beam focus and perpendicular to its axis. Dropping terms in the result of order ϵ^6 and smaller, one gets

$$P[\text{TW}] = \frac{\pi w_0^2}{2} I_0 \left[1 + \frac{\epsilon^2}{4} + \frac{\epsilon^4}{8} \right],$$

$$\approx 0.0216 \left(\frac{q w_0}{\lambda} \right)^2 \left[1 + \frac{\epsilon^2}{4} + \frac{\epsilon^4}{8} \right], \quad (46)$$

where $I_0 = I(0,0,0) = cE_0^2/8\pi$ is the peak intensity (at the focus). Equation (46) clearly shows that for a fixed laser output power, the peak intensity is inversely proportional to the square of the beam waist radius, or equivalently q is inversely proportional to w_0 . Note that Eq. (46) has already been used to compute the q value employed in Figs. 2–5.

For the crossed-beam acceleration scheme two sets of fields are needed, one for each beam with subscripts 1 and 2 used to distinguish their parameter values and propagation characteristics. The resultant field components then enter into the equations of motion (6) in the form

$$E_x = (E_{1x} - E_{2x}) \cos \theta + (E_{1z} - E_{2z}) \sin \theta, \quad (47)$$

$$E_y = E_{1y} - E_{2y}, \quad (48)$$

$$E_z = -(E_{1x} + E_{2x}) \sin \theta + (E_{1z} + E_{2z}) \cos \theta. \quad (49)$$

Similarly,

$$B_x = (B_{1z} - B_{2z}) \sin \theta, \quad (50)$$

$$B_y = B_{1y} - B_{2y}, \quad (51)$$

$$B_z = (B_{1z} + B_{2z}) \cos \theta. \quad (52)$$

Retention of terms of order ϵ and higher in the field expressions brings about corrections which can be quite important when ultrahigh-intensity laser systems are employed. For the business of acceleration the corrections to the electric field terms affect the energy gain directly through the $\boldsymbol{\beta} \cdot \mathbf{E}$ term in the second of Eqs. (6), while corrections to the magnetic field components play an indirect role via the $\boldsymbol{\beta} \times \mathbf{B}$ term in the first equation. We have recently demonstrated [46,47] that focusing down to a waist radius of a few microns requires inclusion of all corrections, i.e., up to and including the ϵ^5 terms. Previous calculations for the crossed-beam configuration [1–4] have at most included the term of order ϵ .

The remainder of this section will be devoted to the discussion of a number of issues related to the acceleration scheme and based upon numerical calculations using the full fields. Obviously, solutions based on low-order perturbation theory [48] cannot be relied upon, considering the high-intensity fields we are concerned with in this work. We will assume that the two beams have the same intensity and frequency, that their propagation directions and field components point as shown in Fig. 8(a), and that they have a common stationary focus at O. The electron will be assumed to

be injected at $t=0$ from a point with coordinates (x_0, y_0, z_0) . β_0 will be used to denote the magnitude of the electron's initial scaled velocity.

B. A preferred crossing angle

Continued improvements in the technology of optical components [4] capable of withstanding present-day laser field intensities [9–11] have motivated us to explore domains of high q and θ values. Guided by the analytic work developed in Sec. II and Fig. 3 we have found that, corresponding to a given set of laser parameters and electron initial conditions, a crossing angle exists that renders the energy gain, due to interaction with a given number of field cycles, a maximum. This is apparently made possible by constructive interference of the two beams.

Figure 3 seems to suggest that, if the electron-field interaction is to terminate in the neighborhood of any one of the points corresponding to $\eta = (2M + 1/2)\pi$, where $M = 0, 1, 2, \dots$, the electron will escape with a maximum energy gain. The gain will be an absolute maximum for $M = 3$ in the \sin^2 pattern case, for example. Confining attention to the situation corresponding to one of these maxima in the energy gain, we have found that a maximum gain is also obtained for a particular crossing angle. In a sense, at this crossing angle, constructive interference of the crossing beams presents the electron with a maximum electric field strength to interact with and absorb energy from. As it turns out, the optimal crossing angle, in the case of acceleration from rest, lends itself to an analytic derivation. So, setting $\eta = (2M + 1/2)\pi$, $\beta_0 = 0$, and $\gamma_0 = 1$ in Eqs. (15) and (20), and extremizing the gain expression with respect to θ , one gets the value

$$\theta_{max} = \tan^{-1} \left[\frac{1}{q} \right], \quad (53)$$

in the plane-wave case. So, the optimal crossing angle can be quite large, in which case the resulting gain would be small, of course.

The equation resulting from extremizing the energy gain is quite complicated in the case of a \sin^2 wave pattern. Thus we opt for showing the preferred crossing angle graphically in Fig. 9 for interaction corresponding to $M=2$, i.e., $\eta = 5\pi/2$. The gain is shown clearly to exhibit an absolute maximum as a function of the crossing angle. Note that, guided by hindsight from Figs. 2 and 3, the case displayed in Fig. 9(b) would have resulted in a duplicate of 9(a) had we opted for a calculation of the gain at $\eta = 13\pi/2$ instead. This choice corresponds to a point close to the focus of the pulsed pattern. It is also interesting to note that a net gain results even when the crossing angle is $\pi/2$ (the counter-propagating beam case).

Figure 9(c) is similar to (a) and (b) but for the Gaussian-beam case. General agreement with the plane-wave analytic predictions is obvious. While the plane-wave analysis exaggerates the gain, it gives a smaller optimum crossing half-angle than does the Gaussian-beam calculation.

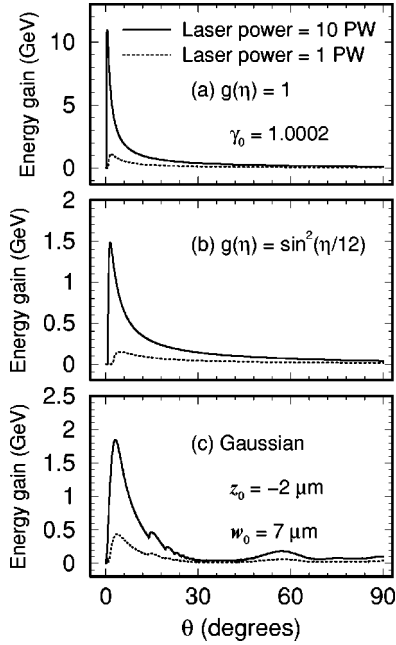


FIG. 9. (a) and (b) Electron energy gain at the end of interaction with 1.25 field cycles (one cycle means $\Delta\eta = 2\pi$) of two beams with the crossing half-angle θ . (c) The same, but for the Gaussian-beam case where motion of the electron is followed for a time equivalent to 10^4 laser field periods (one period here means $T = \lambda/c$). The initial injection energy, $\gamma_0 = 1.0002$, and the legends given in (a) apply everywhere.

In order to get a feeling for what energy gains and energy gradients may be optimally achieved, we have chosen the crossing half-angle $\theta = 3.1^\circ$ for further calculations. This angle lies roughly in a neighborhood of the θ_{max} of Fig. 9(c). Samples of gain vs forward distance results are shown in Fig. 10. Note that the electron-field interaction seems to terminate within 1 mm, for the parameters used. The electron gains more than 1.8 GeV from interaction with the 10 PW beams and over 400 MeV from the 1 PW fields. These gains correspond to the energy gradients 1.8 TeV/m and 0.4 TeV/m, respectively, assuming all the gain occurred over a forward distance of roughly 1 mm.

C. Off-axis parallel injection

Only a small fraction of the electrons in a bunch, of transverse dimensions of a few microns [20], sent along the z axis

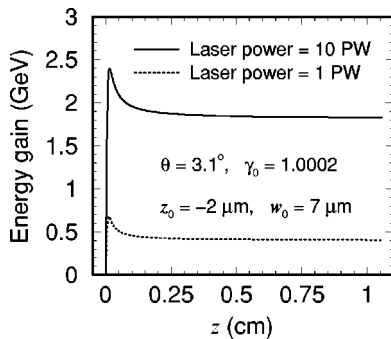


FIG. 10. Energy gain vs the forward distance of travel when the crossing half-angle is $\theta \approx \theta_{max}$ in Fig. 9(c).

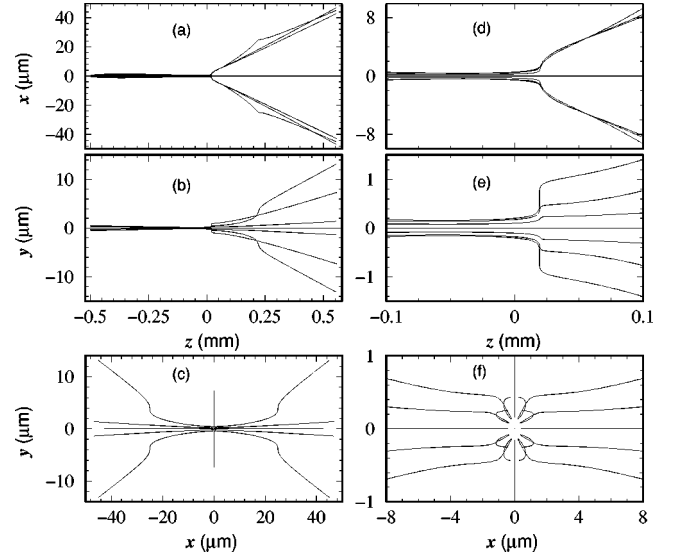


FIG. 11. (a)–(c) Projections, onto the xz , yz , and xy planes, respectively, of the trajectories of 13 electrons injected parallel to the z axis and whose initial coordinates in the xy plane are as follows. One of them starts at the center of a circle of radius $0.5 \mu\text{m}$ and the rest are evenly distributed on the circumference of the same circle, with the first at $(x_0, y_0) = (0.5, 0) \mu\text{m}$, and so on. In (d)–(f) we merely zoom on small portions of (a)–(c), respectively. The remaining parameters are: $\lambda = 1.056 \mu\text{m}$, $w_0 = 7 \mu\text{m}$, $z_0 = -0.5 \mu\text{m}$, $\gamma_0 = 6$, $\theta = 3.1^\circ$, laser power at 1 PW, and interaction time equivalent to 1000 laser periods.

of Fig. 8(a) will typically enter the interaction region with precisely zero initial transverse coordinates. The rest will come in, perhaps parallel to, but a transverse distance from, that axis. In this section, we consider the trajectories of 13 electrons whose initial coordinates in the xy plane are as follows: one is incident perfectly axially, $x_0 = y_0 = 0$; a second has initial xy coordinates $(x_0, y_0) = (0.5, 0) \mu\text{m}$, and the remaining 11 electrons are initially equally spaced on the circumference of a circle in the xy plane of radius $0.5 \mu\text{m}$ and centered on the point $(0, 0, -5) \text{mm}$. These initial coordinates are marked on the circle on the left of Fig. 8(b) and given the labels 0, 1, 2, \dots , 12. The resulting subsequent trajectories are shown in Figs. 11 and 12. The perfect symmetry of the configuration on both sides of the xz plane is reflected in all the trajectories displayed in Figs. 11 and 12, and in the gains in Fig. 13 as well.

Note first the case of electrons whose initial coordinates are confined to the xz plane, those labeled by 1, 0, and 7. Numerical solution of the equations of motion then yield trajectories, in the full fields, that are also confined to that plane. At all points in the xz plane ($y = 0$), the field components E_y and B_z vanish identically at all times. This is easy to see from the geometrical symmetry of the configuration and from the choice of identical beams we have made [or else by setting $y = 0$ in Eqs. (33) and (37)]. With $B_x = 0$, these are the only field components capable of inducing motion out of the xz plane for an electron initially moving in it. Hence three of the above mentioned electrons, those with initial xy coordinates $(0.5, 0)$, $(0, 0)$, and $(-0.5, 0) \mu\text{m}$ and labeled by 1, 0, and 7, respectively, will follow trajectories confined to

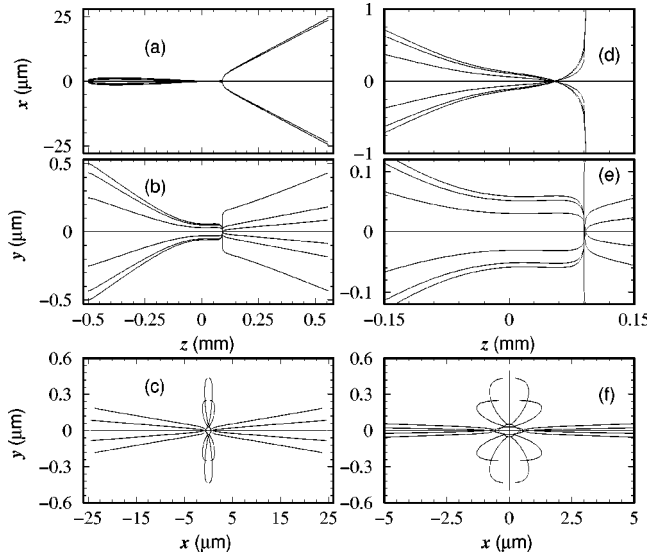


FIG. 12. Same as Fig. 11, but for a laser power of 10 PW.

the xz plane. They make excursions transverse to z whose sizes depend upon the value of x_0 . In particular, axial injection through the point $(x_0, y_0) = (0, 0)$ leads to a perfectly axial trajectory. This trajectory is clearly evident as a straight line in Figs. 11(a)–11(e) and its xy projection appears in Fig. 11(f) as the dot at $(0, 0)$.

Overall, we note that electrons which are injected in the manner just described (over a circle of radius $0.5 \mu\text{m}$) get spread out asymmetrically in the transverse dimensions. The spreading is from $0.5 \mu\text{m}$ to about $40 \mu\text{m}$ in the x direction, and from $0.5 \mu\text{m}$ to a maximum of roughly $14 \mu\text{m}$ in the y direction. A careful look at the trajectory portions displayed in Figs. 11(d)–11(f) reveals clearly that points slightly to the

right of the common focus of the crossed beams act like a strong *scattering center* for the electrons. That neighborhood may be viewed as a *dynamic scattering center*, one that oscillates by responding to the local phase variations of the fields. Conversely, roughly the same neighborhood, for the situation depicted in Fig. 12, acts like a center of attraction causing the trajectories to bend in directions opposite those of Fig. 11. In both cases, however, the electron appears to gain momentum from the fields in the form of a few violent impulses, as evidenced by the sudden kicks along the trajectories shown.

We conclude from Figs. 11 and 12 that, provided the space charge effects are neglected, most electrons in a sub-micro bunch (a bunch of electrons with, say, a circular cross section of transverse radius less than $1 \mu\text{m}$), which is injected initially with its center of mass on the z axis, will follow trajectories that diverge considerably due to the scattering process described above.

Now to answer the question of whether the final energy gain will suffer any spreading as a result of the electrons possessing a spread in the injection positions, we have calculated the gain with axial distances for all cases considered in Figs. 11 and 12. The results are shown in Fig. 13, where the interaction time has been taken as equivalent to 5000 laser periods. Here too, because of the fact that the fields exhibit rapid local phase variations, electrons injected along different initial paths experience drastically different fields. This results in them gaining widely differing amounts of energy as can be seen in Fig. 13(b). In this figure, the above-mentioned 13 electrons gain energies in the approximate range 80–240 MeV. By contrast, one sees in Fig. 13(a), and from examination of the data used to construct it, that the electrons injected through $(x_0, y_0) = (0, 0)$, $(0.5, 0)$, and $(-0.5, 0) \mu\text{m}$ (initial positions corresponding to 0, 4, and 10, respectively) gain about 1.86 GeV. Gain by the remaining electrons is as follows: 1 and 7 gain 1.168 GeV; 2, 6, 8, and 12 gain 1.175; and finally 3, 5, 9, and 11 escape with a net of about 1.193 GeV each. These associations reflect quite clearly the perfect symmetry exhibited by the configuration, and by the fields, on both sides of the xz plane.

D. Effect of injection energy spread

Our theoretical study in this paper has been confined to the single-particle aspects. In a real accelerator design electrons will be injected in bunches of certain characteristics which must be taken into account [20,49].

In this subsection, we calculate the spread in energy gain δW that may result from a spread $\delta \mathcal{E}_0 = mc^2 \delta \gamma_0$ in the injection energy. In the plane-wave case, to begin with, note that $\delta \gamma_0 = \beta_0 \gamma_0^3 \delta \beta_0$. Next, differentiation with respect to β_0 of Eqs. (10), (15), and (20) yields

$$\delta W = \left[(\cos \theta - \beta_0) + \frac{s(1 - \beta_0 \cos \theta)}{\sqrt{s^2 + \sin^2 \theta}} \right] \frac{\delta \mathcal{E}_0}{\beta_0 \sin^2 \theta}, \quad (54)$$

where $s(\eta)$ is given in Eq. (15). Assuming an initial injection energy spread $\delta \mathcal{E}_0 / \mathcal{E}_0 = 0.5\%$ [24], Eq. (54) gives, for

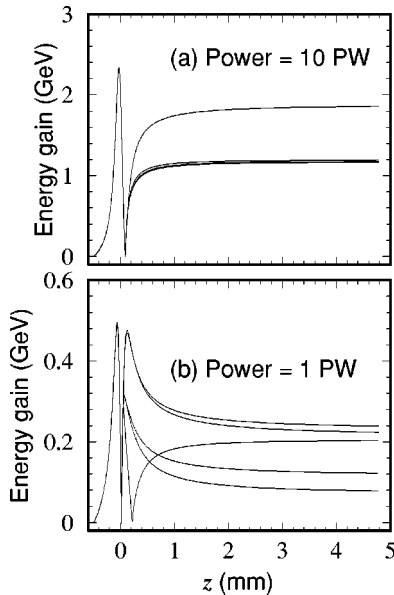


FIG. 13. Electron energy gain as a function of the axial distance for the electrons whose trajectories are given in Figs. 11 and 12. In this figure the interaction time has been taken equivalent to 5000 laser field periods.

electrons ejected at a point corresponding to $\eta = 13\pi/2$ in Fig. 3, $\delta W/W = 0.0042\%$, almost the same for both pulse-shape functions.

A look at Fig. 14 leads to the following conclusion. Slight variations in the initial injection energy lead to enormous jumps in the final resulting gain, as long as those injection energies do not exceed a few MeV. Agreement with the result of the order-of-magnitude calculation made above, however, is good for injection energies in excess of about 5 MeV, due to the saturation alluded to in our comments on Fig. 4 above. These conclusions agree quite well with the numerical calculations employing the full Gaussian-beam fields, as is depicted in Fig. 12. Saturation is seen here to set in for values of γ_0 beyond about 10.

IV. SUMMARY AND CONCLUSIONS

The dynamics of a single electron injected in vacuum through the intersection point of two laser beams has been investigated analytically and numerically. The analytic work resulted in exact working equations for the crossed-beam laser accelerator when the electron is injected axially, i.e., with its initial direction of motion making equal angles with the beam propagation directions. In particular, expressions, in terms of $\eta = \omega(t - z \cos \theta/c)$, for the energy gradient, the energy gain, and the velocity, have been found. Only the final expression for the scattered electron z coordinate has been left with an integral which could be easily performed numerically. The obtained velocity and coordinate expressions were then used to show that the acceleration process may be accompanied by radiative losses. Sample, reasonably precise, emission spectra, containing typically up to 20 harmonics of the laser frequency have been obtained.

In both analytic and numerical investigations the beam crossing angle has been assumed arbitrary; in other words, nowhere has the analysis been restricted to small crossing angles [2,4]. Otherwise, the two beams have been assumed identical as far as their intensities, frequencies, and waist radii are concerned. In the numerical simulations, the fields of a Gaussian beam have been used, where terms of order up to and including ϵ^5 , where ϵ is the beam diffraction angle, have been employed in modeling them.

It can be fairly stated that good qualitative agreement between the simple plane-wave analysis and the precise numerical computations has been established. In particular, both have arrived at the conclusion that, for a given set of field parameters and initial conditions, a crossing angle exists

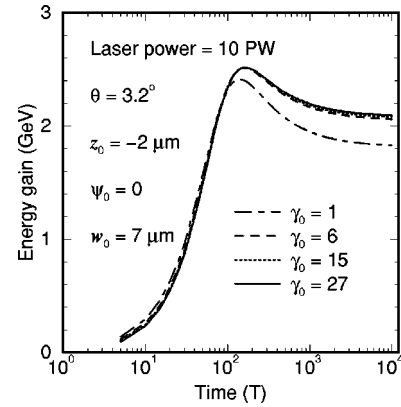


FIG. 14. Electron energy gain as a function of the interaction time, given on a logarithmic scale in terms of the laser period $T = \lambda/c$. The lines shown differ in the initial scaled injection energy and demonstrate saturation with increasing γ_0 at a gain of about 2.1 GeV.

for which gain can be a maximum. Apparently, for such an angle, the electron encounters fields that interfere constructively maximally and favor gain. Furthermore, energy gains of several GeV have been shown to result from interaction with laser beams of present-day PW power.

Our single-particle calculations have also made it possible to arrive at important conclusions regarding the dynamics of an electron bunch in this acceleration scheme. For low-energy electrons (typically less than a few MeV) a small distribution of initial injection energies (or speeds) leads to an enormous distribution of energy gains (or final speeds). Conversely, for electrons incident on the arrangement with high injection energies, the final gains turn out to be hardly sensitive to any spread in those initial injection energies. At high injection energies, the swift energy gain results in the electron reaching an ultrarelativistic speed; it henceforth *rides with the wave* and gains little extra energy. This *saturation* phenomenon implies a limit on the utility of the crossed-beam configuration as a booster accelerator.

ACKNOWLEDGMENTS

Y.I.S. gratefully acknowledges support for this work from the German DAAD Gastdozentenprogramm and the Alexander von Humboldt Stiftung. G.R.M. and C.H.K. are funded by the German Science Foundation (Nachwuchsgruppe within Grant No. SFB 276).

- [1] C.M. Haaland, Opt. Commun. **114**, 280 (1995).
- [2] E. Esarey, P. Sprangle, and J. Krall, Phys. Rev. E **52**, 5443 (1995).
- [3] Y.I. Salamin and C.H. Keitel, Appl. Phys. Lett. **77**, 1082 (2000).
- [4] Y.C. Huang, D. Zheng, W.M. Tulloch, and R.L. Beyer, Appl. Phys. Lett. **68**, 753 (1996); Y.C. Huang and R.L. Beyer, *ibid.* **69**, 2175 (1996); Y.C. Huang and R.L. Beyer, Nucl. Instrum.

Methods Phys. Res. A **407**, 316 (1998); Rev. Sci. Instrum. **69**, 2629 (1998).

- [5] Y.I. Salamin and F.H.M. Faisal, Phys. Rev. A **61**, 043801 (2000).
- [6] Y.I. Salamin, F.H.M. Faisal, and C.H. Keitel, Phys. Rev. A **62**, 053809 (2000).
- [7] Y.I. Salamin and C.H. Keitel, J. Phys. B **33**, 5057 (2000).
- [8] C.P.J. Barty, G. Korn, F. Raksi, C. Rose-Petruck, J. Squier,

- A.-C. Tien, K.R. Wilson, V.V. Yakovlev, and K. Yamakawa, *Opt. Lett.* **21**, 219 (1996).
- [9] D.M. Perry, D. Pennington, and V. Yanovsky, *Opt. Lett.* **24**, 160 (1999).
- [10] S. Backus *et al.*, *Rev. Sci. Instrum.* **69**, 1207 (1998).
- [11] N. Bloembergen, *Rev. Mod. Phys.* **71**, S283 (1999).
- [12] C.W. Domier, N.C. Luhmann, Jr., A.E. Chou, W-M. Zhang, and A.J. Romanowsky, *Rev. Sci. Instrum.* **66**, 399 (1995).
- [13] C. Raman, C.W.S. Conover, C.I. Sukenik, and P.H. Bucksbaum, *Phys. Rev. Lett.* **76**, 2436 (1996).
- [14] A. Bonvalet, M. Joffre, J.L. Martin, and A. Migus, *Appl. Phys. Lett.* **67**, 2907 (1995).
- [15] B. Rau, T. Tajima, and H. Hojo, *Phys. Rev. Lett.* **78**, 3310 (1997).
- [16] X. Wang, Y.K. Ho, Q. Kong, L.J. Zhu, L. Feng, S. Scheid, and H. Hora, *Phys. Rev. E* **58**, 6575 (1998); *ibid.* **60**, 7473 (1999).
- [17] V.P. Kalosha and J. Herrmann, *Phys. Rev. Lett.* **83**, 544 (1999).
- [18] J.D. Lawson, *IEEE Trans. Nucl. Sci.* **NS-26**, 4217 (1979); P.M. Woodward, *J. IEE* **93**, 1554 (1947).
- [19] J. D. Jackson, *Classical Electrodynamics*, 2nd ed. (Wiley, New York, 1975).
- [20] C.P. Neumann, W.S. Graves, and P.G. O'Shea, *Phys. Rev. ST Accel. Beams* **3**, 030701 (2000).
- [21] E.S. Sarachik and G.T. Schappert, *Phys. Rev. D* **1**, 2738 (1970).
- [22] F.V. Hartemann, A.L. Troha, and N.C. Luhmann, Jr., *Phys. Rev. E* **54**, 2956 (1996).
- [23] J.H. Eberly and A. Sleeper, *Phys. Rev.* **176**, 1570 (1968).
- [24] E. Esarey, S.K. Ride, and P. Sprangle, *Phys. Rev. E* **48**, 3003 (1993).
- [25] E. Esarey and P. Sprangle, *Phys. Rev. A* **45**, 5872 (1992).
- [26] S. Varro and F. Ehlötzky, *Z. für Phys. D* **22**, 619 (1992).
- [27] Y.I. Salamin and F.H.M. Faisal, *Phys. Rev. A* **54**, 4383 (1996); *J. Phys. A* **31**, 1319 (1997); *Phys. Rev. A* **55**, 3964 (1997).
- [28] Y.I. Salamin, *Phys. Rev. A* **60**, 3276 (1999).
- [29] Y.I. Salamin and F.H.M. Faisal, *Phys. Rev. A* **58**, 3221 (1998).
- [30] J.-P. Connerade and C.H. Keitel, *Phys. Rev. A* **53**, 2748 (1996).
- [31] M.W. Walser, C. Szymanowski, and C.H. Keitel, *Europhys. Lett.* **48**, 533 (1999).
- [32] M.W. Walser and C.H. Keitel, *J. Phys. B* **33**, L221 (2000).
- [33] C.H. Keitel, P.L. Knight, and K. Burnett, *Europhys. Lett.* **24**, 539 (1993).
- [34] C.H. Keitel, C. Szymanowski, P.L. Knight, and A. Maquet, *J. Phys. B* **31**, L75 (1998).
- [35] Q. Wang and A.F. Starace, *Phys. Rev. A* **55**, 815 (1997).
- [36] M. Bao, I. Fabrikant, and A.F. Starace, *Phys. Rev. A* **58**, 411 (1998).
- [37] D.B. Milošević and A.F. Starace, *Phys. Rev. Lett.* **81**, 5097 (1998).
- [38] N.L. Manakov, V.D. Ovsianikov, and A.F. Starace, *Phys. Rev. Lett.* **82**, 4791 (1999).
- [39] Q. Su, B.A. Smetanko, and R. Grobe, *Opt. Express* **2**, 277 (1998).
- [40] R.E. Wagner, Q. Su, and R. Grobe, *Phys. Rev. A* **60**, 3233 (1999).
- [41] L.W. Davis, *Phys. Rev. A* **19**, 1177 (1979).
- [42] J.P. Barton and D.R. Alexander, *J. Appl. Phys.* **66**, 2800 (1989).
- [43] M.O. Scully and M.S. Zubairy, *Phys. Rev. A* **44**, 2656 (1991).
- [44] K.T. McDonald, www.hep.princeton.edu/~mcdonald/accel/gaussian.ps; www.hep.princeton.edu/~mcdonald/accel/gaussian2.ps.
- [45] F.V. Hartemann, J.R. Van Meter, A.L. Troha, E.C. Landahl, N.C. Luhmann, Jr., H.A. Baldis, Atul Gupta, and A.K. Kerman, *Phys. Rev. E* **58**, 5001 (1998).
- [46] Y.I. Salamin and C.H. Keitel, *Phys. Rev. Lett.* **88**, 095005 (2002).
- [47] Y. I. Salamin, G. R. Mocken, and C. H. Keitel, *Phys. Rev. ST Accel. Beams* **5**, 101301 (2002).
- [48] V.V. Apollonov, M.V. Fedorov, A.M. Prokhorov, and A.G. Suzdaltsev, *IEEE J. Quantum Electron.* **28**, 265-271 (1992), and references therein.
- [49] N.E. Andreev, S.V. Kuznetsov, and I.V. Pogorelsky, *Phys. Rev. ST Accel. Beams* **3**, 021301 (2000).